1-2008

Nonlinear Control Strategy for Advanced Vehicle Thermal Management Systmes

John Wagner
Clemson University, jwagner@clemson.edu

M H. Salah
Clemson University

T H. Mitchell
Clemson University

D M. Dawson
Clemson University

Nonlinear Control Strategy for Advanced Vehicle Thermal Management Systems

M. H. Salah[†], T. H. Mitchell[‡], J. R. Wagner, Ph.D., PE[‡], and D. M. Dawson, Ph.D.[†]

Automotive Research Laboratory
Departments of Mechanical[‡] and Electrical[†] Engineering
Clemson University, Clemson, SC 29634-0921
(864) 656-7376, jwagner@clemson.edu

ABSTRACT

Advanced thermal management systems for internal combustion engines can improve coolant temperature regulation and servomotor power consumption by better regulating the combustion process with multiple computer controlled electromechanical components. The traditional thermostat valve, coolant pump, and clutch-driven radiator fan are upgraded with servomotor actuators. When the system components function harmoniously, desired thermal conditions can be accomplished in a power efficient manner. In this paper, a comprehensive nonlinear control architecture is proposed for transient temperature tracking. An experimental system has been fabricated and assembled which features a variable position smart valve, variable speed electric water pump, variable speed electric radiator fan, engine block, and various sensors. In the configured system, the steam-based heat exchanger emulates the heat generated by the engine's combustion process. Representative numerical and experimental results are discussed to demonstrate the functionality of the thermal management system in accurately tracking prescribed temperature profiles and minimizing electrical power consumption.

1. INTRODUCTION

Internal combustion engine active thermal management systems offer enhanced coolant temperature tracking during transient and steady-state operation. Although the conventional automotive cooling system has proven satisfactory for many decades, servomotor controlled cooling components have the potential to reduce the fuel consumption, parasitic losses, and tailpipe emissions (Brace *et al.*, 2001). Advanced automotive cooling systems replace the conventional wax thermostat valve with a variable position smart valve, and replace the mechanical water pump and radiator fan with electric and/or hydraulic driven actuators (Choukroun and Chanfreau, 2001). This later action decouples the water pump and radiator fan from the engine crankshaft. Hence, the problem of having over/under cooling, due to the mechanical coupling, is solved as well as parasitic losses reduced which arose from operating mechanical components at high rotational speeds (Chalgren and Barron, 2003).

An assessment of thermal management strategies for large on-highway trucks and high-efficiency vehicles has been reported by Wambsganss (1999). Chanfreau *et al.* (2001) studied the benefits of engine cooling with fuel economy and emissions over the FTP drive cycle on a dual voltage 42V-12V minivan. Cho *et al.* (2004) investigated a controllable electric water pump in a class-3 medium duty diesel engine truck. It was shown that the radiator size can be reduced by replacing the mechanical pump with an electrical one. Chalgren and Allen (2005) and Chalgren and Traczyk (2005) improved the temperature control, while decreasing parasitic losses, by replacing the conventional cooling system of a light duty diesel truck with an electric cooling system.

To create an efficient automotive thermal management system, the vehicle's cooling system behavior and transient response must be analyzed. Wagner *et al.* (2001, 2002, 2003) pursued a lumped parameter modeling approach and presented multi-node thermal models which estimated internal engine temperature. Eberth *et al.* (2004) created a mathematical model to analytically predict the dynamic behavior of a 4.6L spark ignition engine. To accompany the mathematical model, analytical/empirical descriptions were developed to describe the smart cooling system components. Henry *et al.* (2001) presented a simulation model of powertrain cooling systems for ground vehicles. The model was validated against test results which featured basic system components (*e.g.*, radiator, water pump, surge (return) tank, hoses and pipes, and engine thermal load).

A multiple node lumped parameter-based thermal network with a suite of mathematical models, describing controllable electromechanical actuators, was introduced by Setlur *et al.* (2005) to support controller studies. The proposed simplified cooling system used electrical immersion heaters to emulate the engine's combustion process and servomotor actuators, with

nonlinear control algorithms, to regulate the temperature. In their experiments, the water pump and radiator fan were set to run at constant speeds, while the smart thermostat valve was controlled to track coolant temperature set points. Cipollone and Villante (2004) tested three cooling control schemes (*e.g.*, closed-loop, model-based, and mixed) and compared them against a traditional "thermostat-based" controller. Page *et al.* (2005) conducted experimental tests on a medium-sized tactical vehicle that was equipped with an intelligent thermal management system. The authors investigated improvements in the engine's peak fuel consumption and thermal operating conditions. Finally, Redfield *et al.* (2006) operated a class 8 tractor at highway speeds to study potential energy saving and demonstrate engine cooling to with ±3ºC of a set point value.

In this paper, nonlinear control strategies are presented to actively regulate the coolant temperature in internal combustion engines. An advanced thermal management system has been implemented on a laboratory test bench that featured a smart thermostat valve, variable speed electric water pump and fan, radiator, engine block, and a steam-based heat exchanger to emulate the combustion heating process. The proposed backstepping robust control strategy has been verified by simulation techniques and validated by experimental testing. In Section 2, a set of mathematical models are presented to describe the automotive cooling components and thermal system dynamics. A nonlinear tracking control strategy is introduced in Section 3. Section 4 presents the experimental test bench, while Section 5 introduces numerical and experimental results. The conclusion is contained in Section 6. The Appendices present a Lyapunov-based stability analysis, which is needed for the controller's design, as well as the Nomenclature List.

2. AUTOMOTIVE THERMAL MANAGEMENT MODELS

A suite of mathematical models will be presented to describe the dynamic behavior of the advanced cooling system. The system components include a 6.0L diesel engine with a steam-based heat exchanger to emulate the combustion heat, a three-way smart valve, a variable speed electric water pump, and a radiator with a variable speed electric fan.

2.1 Cooling System Thermal Descriptions

A reduced order two-node lumped parameter thermal model (refer to Figure 1) describes the cooling system's transient response and minimizes the computational burden for in-vehicle implementation. The engine block and radiator behavior can be described by

$$C_e \dot{T}_e = Q_{in} - C_{pc} \dot{m}_r \left(T_e - T_r \right) \tag{1}$$

$$C_r \dot{T}_r = -Q_o + C_{pc} \dot{m}_r \left(T_e - T_r \right) - \varepsilon C_{pa} \dot{m}_f \left(T_e - T_\infty \right). \tag{2}$$

The variable Q_{in} and Q_o represent the input heat generated by the combustion process and the radiator heat loss due to uncontrollable air flow, respectively. An adjustable double pass steam-based heat exchanger delivers the emulated heat of combustion at a maximum 55kW in a controllable and repeatable manner. In an actual vehicle, the combustion process will generate this heat which is transferred to the coolant through the block's water jacket.

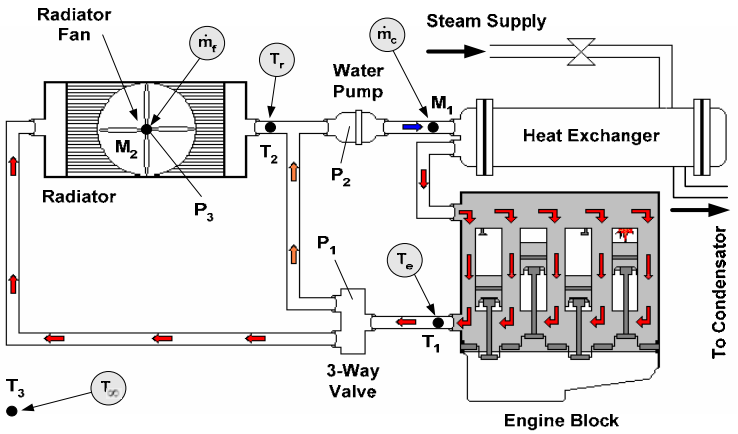

Figure 1: Advanced cooling system which features a smart valve, variable speed pump, variable speed fan, engine block, radiator, and sensors (temperature, mass flow rate, and power)

For a three-way servo-driven thermostat valve, the radiator coolant mass flow rate, $\dot{m}_r(t)$, is based on the pump flow rate and normalized valve position as $\dot{m}_r = H\dot{m}_c$ where the variable $H(t)$ satisfies the condition $0 \le H(t) \le 1$. Note that $H(t) = 1(0)$ corresponds to a fully closed (open) valve position and coolant flow through the radiator (bypass) loop. To facilitate the controller design process, three assumptions are imposed:

A1: *The signals $Q_{in}(t)$ and $Q_o(t)$ always remain positive in (1) and (2) (i.e., $Q_{in}(t), Q_o(t) \ge 0$). Further, the signals $Q_{in}(t)$ and $Q_o(t)$, and their first two time derivatives remain bounded at all time, such that $Q_{in}(t), \dot{Q}_{in}(t), \ddot{Q}_{in}(t), Q_o(t), \dot{Q}_o(t), \ddot{Q}_o(t) \in L_\infty$.*

A2: *The surrounding ambient temperature $T_\infty(t)$ is uniform and satisfies $T_e(t) - T_\infty(t) \ge \varepsilon_1, \forall t \ge 0$ where $\varepsilon_1 \in \Re^+$ is a constant.*

A3: *The engine block and radiator temperatures satisfy the condition $T_e(t) - T_r(t) \ge \varepsilon_2, \forall t \ge 0$ where $\varepsilon_2 \in \Re^+$ is a constant. Further, $T_e(0) \ge T_r(0)$ to facilitate the boundedness of signal argument.*

This final assumption allows the engine and radiator to initially be the same temperature (e.g., cold start). The unlikely case of $T_e(0) < T_r(0)$ is not considered.

2.2 Variable Position Smart Valve

A dc servo-motor has been actuated in both directions to operate the multi-position smart thermostat valve. The compact motor, with integrated external potentiometer for position feedback, is attached to a worm gear assembly that is connected to the valve's piston. The governing equation for the motor's armature current, i_{av}, can be written as

$$\frac{di_{av}}{dt} = \frac{1}{L_{av}}\left(V_v - R_{av}i_{av} - K_{bv}\frac{d\theta_v}{dt}\right). \tag{3}$$

The motor's angular velocity, $d\theta_v(t)/dt$, may be computed as

$$\frac{d^2\theta_v}{dt^2} = \frac{1}{J_v}\left(-b_v\frac{d\theta_v}{dt} + K_{mv}i_{av} + 0.5dN.\left(A_p\Delta P + c\,\mathrm{sgn}\left(\frac{dh}{dt}\right)\right)\right). \tag{4}$$

Note that the motor is operated by a high gain proportional control to reduce the position error and speed up the overall piston response.

2.3 Variable Speed Water Pump

A computer controlled electric motor operates the high capacity centrifugal water pump. The motor's armature current, i_{ap}, can be described as

$$\frac{di_{ap}}{dt} = \frac{1}{L_{ap}}\left(V_p - R_{ap} i_{ap} - K_{bp}\omega_p\right) \tag{5}$$

where the motor's angular velocity, $\omega_p(t)$, can be computed as

$$\frac{d\omega_p}{dt} = \frac{1}{J_p}\left(-\left(b_p + R_f V_o^2\right)\omega_p + K_{mp} i_{ap}\right). \tag{6}$$

The coolant mass flow rate for a centrifugal water pump depends on the coolant density, shaft speed, system geometry, and pump configuration. The mass flow rate may be computed as $\dot{m}_c = \rho_c(2\pi r b v)$ where $v(t) = (r\omega_p)\tan\beta$. It is assumed that the inlet radiator velocity, $v(t)$, is equal to the inlet fluid velocity and that the flow enters normal to the impeller.

2.4 Variable Speed Radiator Fan

A cross flow heat exchanger and a dc servo-motor driven fan form the radiator assembly. The electric motor directly drives a multi-blade fan that pulls the surrounding air through the radiator assembly. The air mass flow rate going through the radiator is affected directly by the fan's rotational speed, ω_f, so that

$$\frac{d\omega_f}{dt} = \frac{1}{J_f}\left(-b_f\omega_f + K_{mf} i_{af} - \rho_a A_f R_f V_{af}^2\right) \tag{7}$$

where $V_{af} = \left(\left(K_{mf} / \eta_f \rho_a A_f\right) i_{af} \omega_f\right)^{0.3}$. The corresponding air mass flow rate is written as $\dot{m}_f = \beta_r \rho_a A_f V_{af} + \dot{m}_{ram}$. The last term denotes the ram air mass flow rate effect due to vehicle speed or ambient wind velocity. The fan motor's armature current, i_{af}, can be described as

$$\frac{di_{af}}{dt} = \frac{1}{L_{af}}\left(V_f - R_{af} i_{af} - K_{bf} \omega_f\right). \tag{8}$$

Note that a voltage divider circuit has been inserted into the experimental system to measure the current drawn by the fan and estimate the power consumed.

3. THERMAL SYSTEM CONTROL DESIGN

A Lyapunov-based nonlinear control algorithm will be presented to maintain a desired engine block temperature, $T_{ed}(t)$. The controller's main objective is to precisely track engine temperature set points while compensating for system uncertainties (i.e., combustion process input heat, $Q_{in}(t)$, radiator heat loss, $Q_o(t)$) by harmoniously controlling the system actuators. Referring to Figure 1, the system servo-actuators are a three-way smart valve, a water pump, and a radiator fan. Another important objective is to reduce the electric power consumed by these actuators, $P_M(t)$. The main concern is pointed towards the fact that the radiator fan consumes the most power of all cooling system components followed by the pump. It is also important to point out that in (1) and (2), the signals $T_e(t)$, $T_r(t)$ and $T_\infty(t)$ can be measured by either thermocouples or thermistors, and the system parameters C_{pc}, C_{pa}, C_e, C_r, and ε are assumed to be constant and fully known.

3.1 Backstepping Robust Control Objective

The control objective is to ensure that the actual temperatures of the engine, $T_e(t)$, and the radiator, $T_r(t)$, track the desired trajectories $T_{ed}(t)$ and $T_{vr}(t)$,

$$\left|T_{ed}(t)-T_e(t)\right| \le \varepsilon_e,\ \left|T_r(t)-T_{vr}(t)\right| \le \varepsilon_r \ \text{ as } \ t \to \infty \tag{9}$$

while compensating for the system variable uncertainties $Q_{in}(t)$ and $Q_o(t)$ where ε_e and ε_r are positive constants.

A4: *The engine temperature profiles are always bounded and chosen such that their first three time derivatives remain bounded at all times (i.e.,* $T_{ed}(t), \dot{T}_{ed}(t), \ddot{T}_{ed}(t)$ *and* $\dddot{T}_{ed}(t) \in L_\infty$*). Further,* $T_{ed}(t) >> T_\infty$ *at all times.*

Remark 1: *Although it is unlikely that the desired radiator temperature setpoint,* $T_{vr}(t)$*, is required (or known) by the automotive engineer, it will be shown that the radiator setpoint can be indirectly designed based on the engine's thermal conditions and commutation strategy (refer to Remark 2).*

To facilitate the controller's development and quantify the temperature tracking control objective, the tracking error signals $e(t)$ and $\eta(t)$ are defined as

$$e \triangleq T_{ed} - T_e,\ \eta \triangleq T_r - T_{vr} \tag{10}$$

By adding and subtracting $MT_{vr}(t)$ to (1), and expanding the variables $M = C_{pc} m_o$ and $\dot{m}_r(t) = m_o + \bar{m} = H_o \dot{m}_c + \bar{H}\dot{m}_c$, the engine and radiator dynamics can be rewritten as

$$C_e \dot{T}_e = Q_{in} - M\left(T_e - T_{vr}\right) - C_{pc}\bar{m}\left(T_e - T_r\right) + M\eta \tag{11}$$

$$C_r \dot{T}_r = -Q_o + C_{pc}\left(m_o + \bar{m}\right)\left(T_e - T_r\right) - \varepsilon C_{pa}\dot{m}_f\left(T_e - T_\infty\right) \tag{12}$$

where $\eta(t)$ was introduced in (10), and m_o and H_o are positive design constants.

3.2 Closed-Loop Error System Development and Controller Formulation

The open-loop error system can be analyzed by taking the first time derivative of both expressions in (10) and then multiplying both sides of the resulting equations by C_e and C_r for the engine and radiator dynamics, respectively. Thus, the system dynamics described in (11) and (12) can be substituted and then reformatted to realize

$$C_e \dot{e} = C_e \dot{T}_{ed} - Q_{in} + M\left(T_e - T_{vro}\right) - u_e - M\eta \tag{13}$$

$$C_r\dot{\eta} = M\left(T_e - T_r\right) - Q_o + u_r - C_r\dot{T}_{vr} \tag{14}$$

In these expressions, (10) was utilized as well as $T_{vr}(t) \triangleq T_{vro} + \bar{T}_{vr}$, $u_e(t) = M\bar{T}_{vr} - C_{pc}\bar{m}\left(T_e - T_r\right)$, and $u_r(t) = C_{pc}\bar{m}\left(T_e - T_r\right) - \varepsilon C_{pa}\dot{m}_f\left(T_e - T_\infty\right)$. The parameter T_{vro} is a positive design constant.

Remark 2: *The control inputs $\bar{m}(t)$, $\bar{T}_{vr}(t)$ and $\dot{m}_f(t)$ are uni-polar. Hence, commutation strategies are designed to implement the bi-polar inputs $u_e(t)$ and $u_r(t)$ as*

$$\bar{m} \triangleq \frac{u_e\left[\operatorname{sgn}\left(u_e\right)-1\right]}{2C_{pc}\left(T_e - T_r\right)}, \qquad \bar{T}_{vr} \triangleq \frac{u_e\left[1+\operatorname{sgn}\left(u_e\right)\right]}{2M}, \qquad \dot{m}_f \triangleq \frac{F\left[1+\operatorname{sgn}\left(F\right)\right]}{2\varepsilon C_{pa}\left(T_e - T_\infty\right)} \tag{15}$$

where $F(t) \triangleq C_{pc}\bar{m}\left(T_e - T_r\right) - u_r$. The control input, $\dot{m}_f(t)$ is obtained from (15) after $\bar{m}(t)$ is computed. From these definitions, it is clear that if $u_e(t), u_r(t) \in L_\infty \forall t \geq 0$, then $\bar{m}(t), \bar{T}_{vr}(t), \dot{m}_f(t) \in L_\infty \forall t \geq 0$.

To facilitate the subsequent analysis, the expressions in (13) and (14) are rewritten as

$$C_e\dot{e} = \tilde{N}_e + N_{ed} - u_e - M\eta, \qquad C_r\dot{\eta} = \tilde{N}_r + N_{rd} + u_r - C_r\dot{T}_{vr} \tag{16}$$

where the auxiliary signals $\tilde{N}_e(T_e, t)$ and $\tilde{N}_r(T_e, T_r, t)$ are defined as

$$\tilde{N}_e \triangleq N_e - N_{ed}, \qquad \tilde{N}_r \triangleq N_r - N_{rd}. \tag{17}$$

Further, the signals $N_e(T_e, t)$ and $N_r(T_e, T_r, t)$ are defined as

$$N_e \triangleq C_e\dot{T}_{ed} - Q_{in} + M\left(T_e - T_{vro}\right), \qquad N_r \triangleq M\left(T_e - T_r\right) - Q_o \tag{18}$$

with both $N_{ed}(t)$ and $N_{rd}(t)$ represented as

$$N_{ed} \triangleq N_e\Big|_{T_e = T_{ed}} = C_e\dot{T}_{ed} - Q_{in} + M\left(T_{ed} - T_{vro}\right), \qquad N_{rd} \triangleq N_r\Big|_{T_e = T_{ed}, T_r = T_{vr}} = M\left(T_{ed} - T_{vr}\right) - Q_o. \tag{19}$$

Based on (17) through (19), the control laws $u_e(t)$ and $u_r(t)$ introduced in (16) are designed as

$$u_e = K_e e, \qquad u_r = -K_r\eta + \bar{u}_r \tag{20}$$

where $\bar{u}_r(t)$ is selected as

$$\bar{u}_r = \begin{Bmatrix} 2Me, & \forall u_e \in (-\infty, 0) \\ \left(2M - K_e\dfrac{C_r}{C_e} - \dfrac{C_rK_e^2}{C_eM}\right)e - \dfrac{C_rK_e}{C_e}\eta, & \forall u_e \in [0, \infty) \end{Bmatrix}. \tag{21}$$

Knowledge of $u_e(t)$ and $u_r(t)$, based on (20) and (21), allows the commutation relationships of (15) to be calculated which provides $\dot{m}_r(t)$ and $\dot{m}_f(t)$. Finally, the voltage signals for the pump and fan are prescribed using $\dot{m}_r(t)$ and $\dot{m}_f(t)$ with *a priori* empirical relationships.

3.3 Stability Analysis

A Lyapunov-based stability analysis guarantees that the advanced thermal management system will be stable when applying the control laws introduced in (20) and (21).

Theorem 1: *The controller given in (20) and (21) ensures that: (i) all closed-loop signals stay bounded for all time; and (ii) tracking is uniformly ultimately bounded (UUB) in the sense that ($|e(t)| \le \varepsilon_e, |\eta(t)| \le \varepsilon_r$ as $t \to \infty$).*

Proof: *See Appendix A for the complete Lyapunov-based stability analysis.*

3.4 Normal Radiator Operation Strategy

The electric radiator fan must be controlled harmoniously with the other thermal management system actuators to ensure proper power consumption. From the backstepping robust control strategy, a virtual reference for the radiator temperature, $T_{vr}(t)$, is designed to facilitate the radiator fan control law (refer to Remark 1). A tracking error signal, $\eta(t)$, is introduced for the radiator temperature. Based on the radiator's mathematical description in (2), the radiator may operate normally, as a heat exchanger, if the effort of the radiator fan $\varepsilon C_{pa}\dot{m}_f(T_e - T_\infty)$, donated by $u_r(t)$ in (22), is set to equal the effort produced by the water pump $C_{pc}\dot{m}_r(T_e - T_r)$, donated by $u_e(t)$ in (23). Therefore, the control input $u_e(t)$ provides the signals $\dot{m}_r(t)$ and $\dot{m}_f(t)$.

To derive the operating strategy, the system dynamics (1) and (2) can be written as

$$C_e\dot{T}_e = Q_{in} - u_e \tag{22}$$

$$C_r\dot{T}_r = -Q_o + u_e - u_r . \tag{23}$$

If $u_r(t)$ is selected so that it equals $u_e(t)$, then the radiator operates normally. The control input $u_e(t)$ can be designed, utilizing a Lyapunov-based analysis, to robustly regulate the temperature of the engine block as

$$u_e = -(K_e + \alpha_e)[e - e_o] - \int_{t_o}^{t} \left[\alpha_e (K_e + \alpha_e) e(\tau) + \rho_e \operatorname{sgn}(e(\tau))\right] d\tau \tag{24}$$

where the last term in (24) compensates for the variable unmeasurable input heat, $Q_{in}(t)$. Refer to Setlur *et al.* (2005) for more details on this robust control design method.

Remark 3: *The control input $\dot{m}_r(t)$ is uni-polar. Again, a commutation strategy may be designed to implement the bi-polar input $u_e(t)$ as*

$$\dot{m}_r \triangleq \frac{u_e\left[1 + \operatorname{sgn}(u_e)\right]}{2C_{pc}(T_e - T_r)}. \tag{25}$$

From this definition, if $u_e(t) \in L_\infty \forall t \geq 0$, then $\dot{m}_r(t) \in L_\infty \forall t \geq 0$. The choice of the valve position and water pump's speed to produce the required control input $\dot{m}_r(t)$, defined in (25), can be determined based on energy optimization issues. Further, this allows $\dot{m}_r(t)$ to approach zero without stagnation of the coolant since $\dot{m}_r = H\dot{m}_c$ and $0 \leq H(t) \leq 1$. Another commutation strategy is needed to compute the uni-polar control input $\dot{m}_f(t)$ so that

$$\dot{m}_f \triangleq \frac{u_r\left[1 + \operatorname{sgn}(u_r)\right]}{2\varepsilon C_{pa}(T_e - T_\infty)} \tag{26}$$

where $u_r(t) = u_e(t)$. From this definition, if $u_r(t) \in L_\infty \forall t \geq 0$, then $\dot{m}_f(t) \in L_\infty \forall t \geq 0$.

4. THERMAL TEST BENCH

An experimental test bench (refer to Figure 2) has been fabricated to demonstrate the proposed advanced thermal management system controller design. The assembled test bench offers a flexible, rapid, repeatable, and safe testing environment. Clemson University facilities generated steam is utilized to rapidly heat the coolant circulating within the cooling system via a two-pass shell and tube heat exchanger. The heated coolant is then routed through a 6.0L diesel engine block to emulate the combustion process heat. From the engine block, the coolant flows to a three-way smart valve and then either through the bypass or radiator to the water pump to

close the loop. The thermal response of the engine block to the adjustable, externally applied heat source emulates the heat transfer process between the combustion gases, cylinder wall, and water jacket in an actual operating engine. As shown in Figure 1, the system sensors include three type-J thermocouples (e.g., T_1 = engine temperature, T_2 = radiator temperature, and T_3 = ambient temperature), two mass flow meters (e.g., M_1 = coolant mass flow meter, and M_2 = air mass flow meter), and electric voltage and current measurements (e.g., P_1 = valve power consumed, P_2 = pump power consumed, and P_3 = fan power consumed).

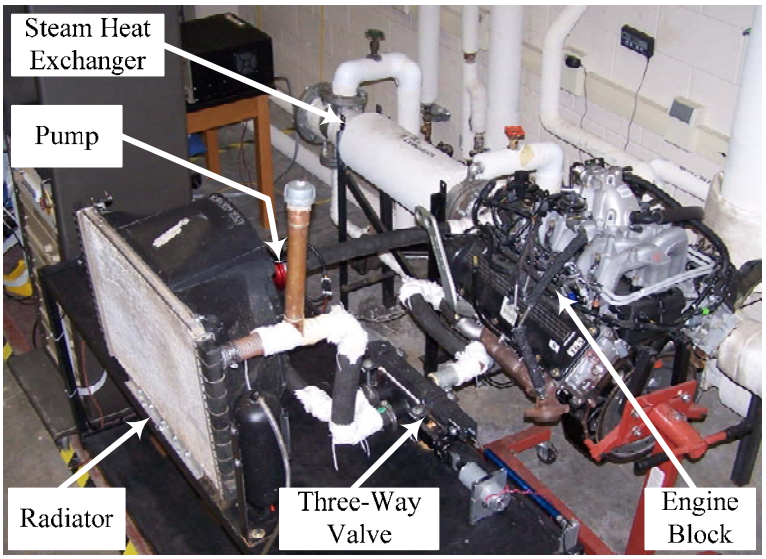

Figure 2: Experimental thermal test bench that features a 6.0L diesel engine block, three-way smart valve, electric water pump, electric radiator fan, radiator, and steam-based heat exchanger

The steam bench can provide up to 55 kW of energy. High pressure saturated steam (412 kPa) is routed from the campus facilities plant to the steam test bench, where a pressure regulator reduces the steam pressure to 172 kPa before it enters the low pressure filter. The low pressure saturated steam is then routed to the double pass steam heat exchanger to heat the system's coolant. The amount of energy transferred to the system is controlled by the main valve mounted on the heat exchanger. The mass flow rate of condensate is proportional to the energy transfer to the circulating coolant. Condensed steam may be collected and measured to calculate the rate of

energy transfer. From steam tables, the enthalpy of condensation can be acquired. To facilitate the analysis, pure saturated steam and condensate at approximately T=100ºC determines the enthalpy of condensation. Baseline testing was performed to determine the average energy transferred to the coolant at various steam control valve positions. The coolant temperatures were initialized at T_e = 67ºC before measuring the condensate. Each test was executed for different time periods.

5. NUMERICAL AND EXPERIMENTAL RESULTS

In this section, the numerical and experimental results are presented to verify and validate the mathematical models and control design. First, a set of Matlab/Simulink™ simulations have been created and executed to evaluate the backstepping robust control design and the normal radiator operation strategy. The proposed thermal model parameters used in the simulations are C_e = 17.14kJ/ºK, C_r = 8.36kJ/ºK, C_{pc} = 4.18kJ/kg.ºK, C_{pa} = 1kJ/kg.ºK, ε = 0.6, and $T_\infty(t)$ = 293ºK. Second, a set of experimental tests have been conducted on the steam-based thermal test bench to investigate the control design and operation strategies.

3.5 Backstepping Robust Control

A numerical simulation of the backstepping robust control strategy, introduced in Section 3, has been performed on the system dynamics (1) and (2) to demonstrate the performance of the proposed controller in (20) and (21). For added reality, band-limited white noise was added to the plant. To simplify the subsequent analysis, a fixed smart valve position of $H(t)=1$ (e.g., fully closed for 100% radiator flow) has been applied to investigate the water pump's ability to regulate the engine temperature. An external ram air disturbance was introduced to emulate a vehicle traveling at 20km/h with varying input heat of $Q_{in}(t)=$[50kW, 40kW, 20kW, 35kW] as

shown in Figure 3. The initial simulation conditions were $T_e(0) = 350\,^{o}\text{K}$ and $T_r(0) = 340\,^{o}\text{K}$. The control design constants are $T_{vro} = 356\,^{o}\text{K}$ and $m_o = 0.4$. Similarly, the controller gains were selected as $K_e = 40$ and $K_r = 0.005$. The desired engine temperature varied as $T_{ed}(t) = 363 + \sin(0.05t)\,^{o}\text{K}$. This time varying setpoint allows the controller's tracking performance to be studied.

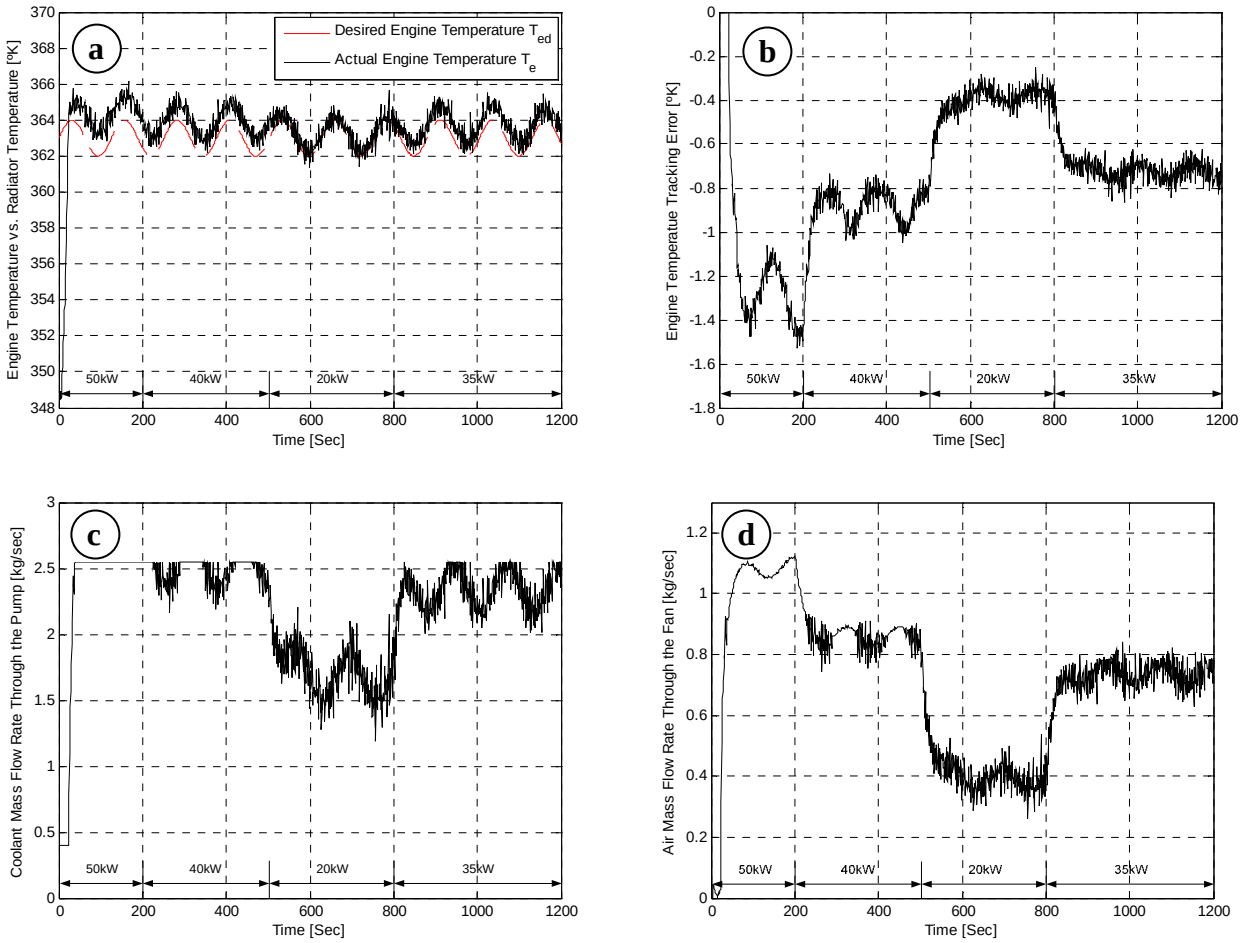

Figure 3: Numerical response of the backstepping robust controller for variable engine thermal loads. (a) Simulated engine temperature response for desired engine temperature profile $T_{ed}(t) = 363 + \sin(0.05t)\,^{o}\text{K}$; (b) Simulated engine commanded temperature tracking error; (c) Simulated mass flow rate through the pump; and (d) Simulated air mass flow rate through the radiator fan.

In Figure 3a, the backstepping robust controller readily handles the heat fluctuations in the system at t = [200sec, 500sec, 800sec]. For instance, when $Q_{in}(t) = 50\text{kW}$ (heavy thermal load) is applied from $0 \le t \le 200\,\text{sec}$, as well as when $Q_{in}(t) = 20\text{kW}$ (light thermal load) is applied at $500 \le t \le 800\,\text{sec}$, the controller is able to maintain a maximum absolute value tracking error of 1.5ºK. Under the presented operating condition, the error in Figure 3b fluctuates between –0.4ºK and –1.5ºK. In Figures 3c and 3d, the coolant pump (maximum flow limit of 2.6kg/sec) works harder than the radiator fan which is ideal for power minimization.

Remark 4: *The error fluctuation in Figure 3b is quite good when compared to the overall amount of heat handled by the cooling system components.*

Two scenarios have been implemented to investigate the controller's performance on the experimental test bench. The first case applies a fixed input heat of $Q_{in}(t) = 35\text{kW}$ and a ram air disturbance which emulates a vehicle traveling at 20km/h as shown in Figure 4. From Figure 4b, the controller can achieve a steady state absolute value temperature tracking error of 0.7ºK. In Figures 4c and 4d, the water pump works harder than the radiator fan which again is ideal for power minimization. Note that the water pump reaches its maximum mass flow rate of 2.6kg/sec, and that the fan runs at 73% of its maximum speed (e.g., maximum air mass flow rate is 1.16kg/sec). The fluctuation in the coolant and air mass flow rates during $0 \le t \le 400\,\text{sec}$ (refer to Figures 4c and 4d) is due to the fluctuation in the actual radiator temperature about the radiator temperature virtual reference $T_{vro}(t) = 356\text{ºK}$ as shown in Figure 4a.

The second scenario varies both the input heat and disturbance. Specifically $Q_{in}(t)$ changes from 50kW to 35kW at t = 200sec while $Q_o(t)$ varies from 20km/h to 40km/h to 20km/h at t =400sec and 700sec (refer to Figure 5). From Figure 5b, it is clear that the proposed control strategy handles the input heat and ram air variations nicely. During the ram air variation

between 550sec and 750sec, the temperature error fluctuates within 1ºK due to the oscillations in the water pump and radiator fan flow rates per Figures 5c and 5d. This behavior may be attributed to the supplied ram air that causes the actual radiator temperature, $T_r(t)$, to fluctuate about the radiator temperature virtual reference $T_{vro}(t) = 356$ºK in Figure 5a.

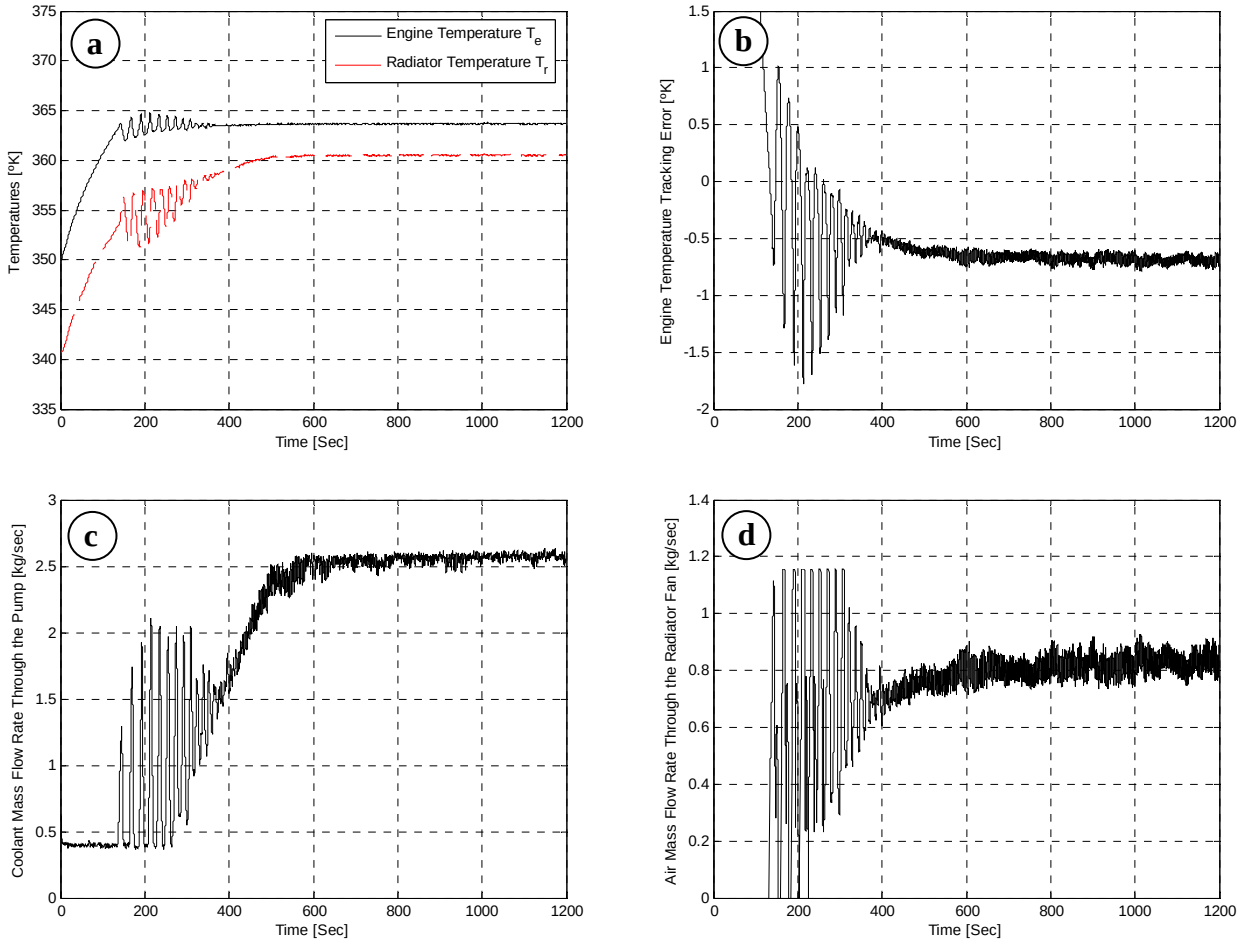

Figure 4: First experimental test for the backstepping robust controller with emulated vehicle speed of 20km/h and $Q_{in}(t) = 35$ kW. (a) Experimental engine and radiator temperatures with a desired engine temperature $T_{ed}(t) = 363$ ºK; (b) Experimental engine temperature tracking error; (c) Experimental coolant mass flow rate through the pump; and (d) Experimental air mass flow rate through the radiator fan.

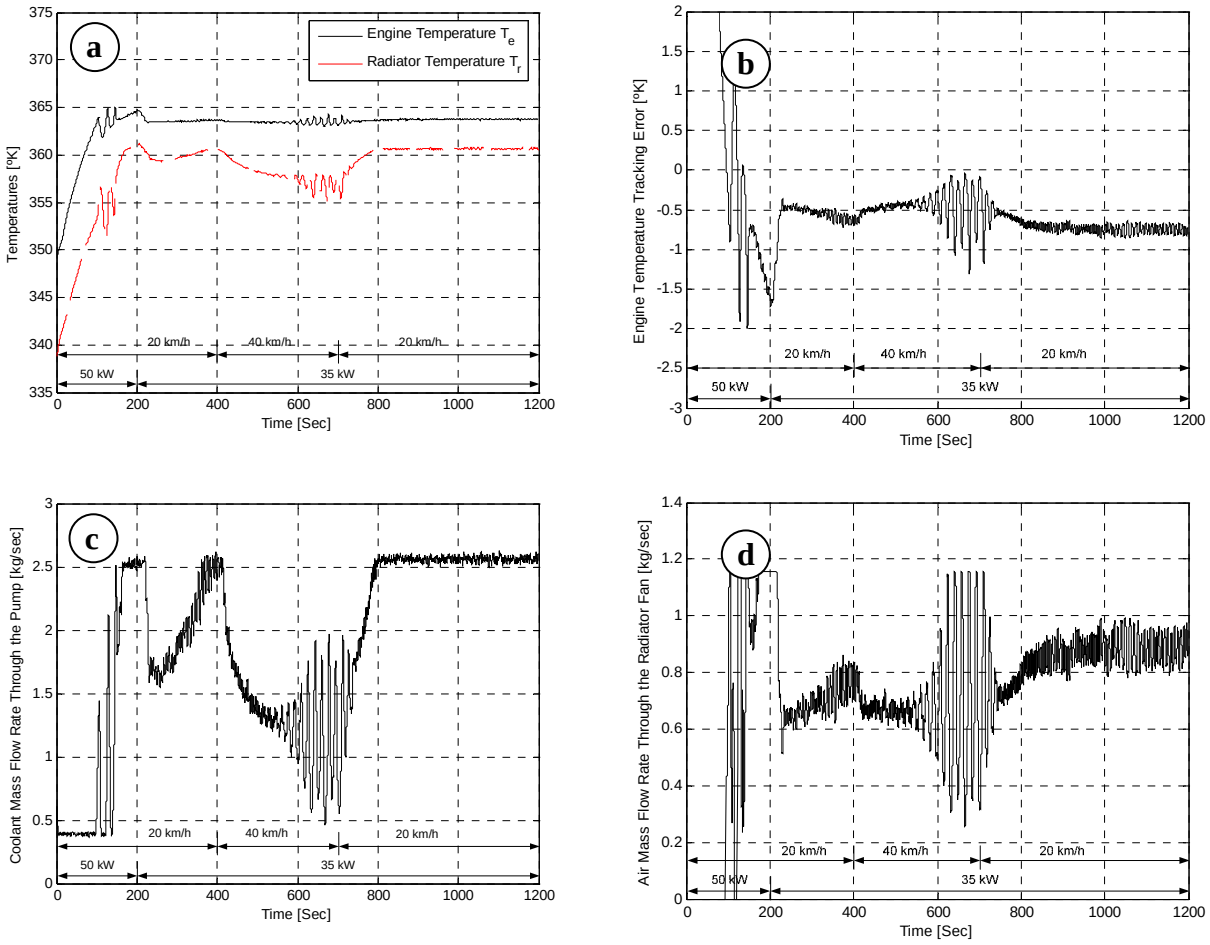

Figure 5: Second experimental test scenario for the backstepping robust controller where the input heat and ram air disturbance vary with time. (a) Experimental engine and radiator temperatures with a desired engine temperature $T_{ed}(t) = 363\,^{o}\mathrm{K}$; (b) Experimental engine temperature tracking error; (c) Experimental coolant mass flow rate through the pump; and (d) Experimental air mass flow rate through the radiator fan.

3.6 Normal Radiator Operation Strategy

The normal radiator operation strategy, introduced in Section 3, has been numerically simulated using system dynamics (1) and (2) to investigate the robust tracking controller performance given in (24). The simulated thermal system's parameters, initial simulation conditions, and desired engine temperature were equivalent to Section 5.1. Again, a band-limited white noise was added to the plant. A fixed 100% radiator flow smart valve position allows the water pump's ability to regulate the engine temperature to be studied. The external ram air

emulated a vehicle traveling at 20km/h; the input heat was varied as shown in Figure 6 (e.g., $Q_{in}(t) = [50\text{kW}, 40\text{kW}, 20\text{kW}, 35\text{kW}]$). The control gains were set as $K_e = 10$, $\alpha_e = 0.005$, and $\rho_e = 0.1$. Although the normal radiator operation accommodated the heat variations in Figure 6a, its performance was inferior to the backstepping robust control. However, the normal radiator operation achieved less tracking error under the same operating condition when Figure 3b and 6b are compared. In this case, the maximum temperature tracking error fluctuation was 1ºK. In Figures 6c and 6d, the pump works harder than the fan which is preferred for power minimization. Note that the power consumption is larger than that achieved by the backstepping robust controller (refer to Figures 3c, 3d, 6c, and 6d).

The same two experimental scenarios presented for the backstepping robust controller are now implemented for the normal radiator operation strategy on the thermal test bench. In the first scenario, a fixed input heat and ram air disturbance, $Q_{in}(t) = 35\text{kW}$ and 20km/h vehicle speed, were applied. In Figure 7a, the normal radiator operation overshoot and settling time are larger than the backstepping robust control (refer to Figure 4a). As shown in Figure 7b, an improved engine temperature tracking error was demonstrated but with greater power consumption in comparison to the backstepping robust control (refer to Figure 4b). Finally, the water pump operated continuously at its maximum per Figure 7c.

For the second test scenario, the input heat and disturbance are both varied as previously described for the backstepping robust control. The normal radiator operation maintained the established control gains. In Figure 8b, the temperature error remains within a ±0.4ºK neighborhood of zero despite variations in the input heat and ram air. Although the temperature tracking error is quite good, this strategy does not minimize power consumption in comparison to the backstepping robust control strategy.

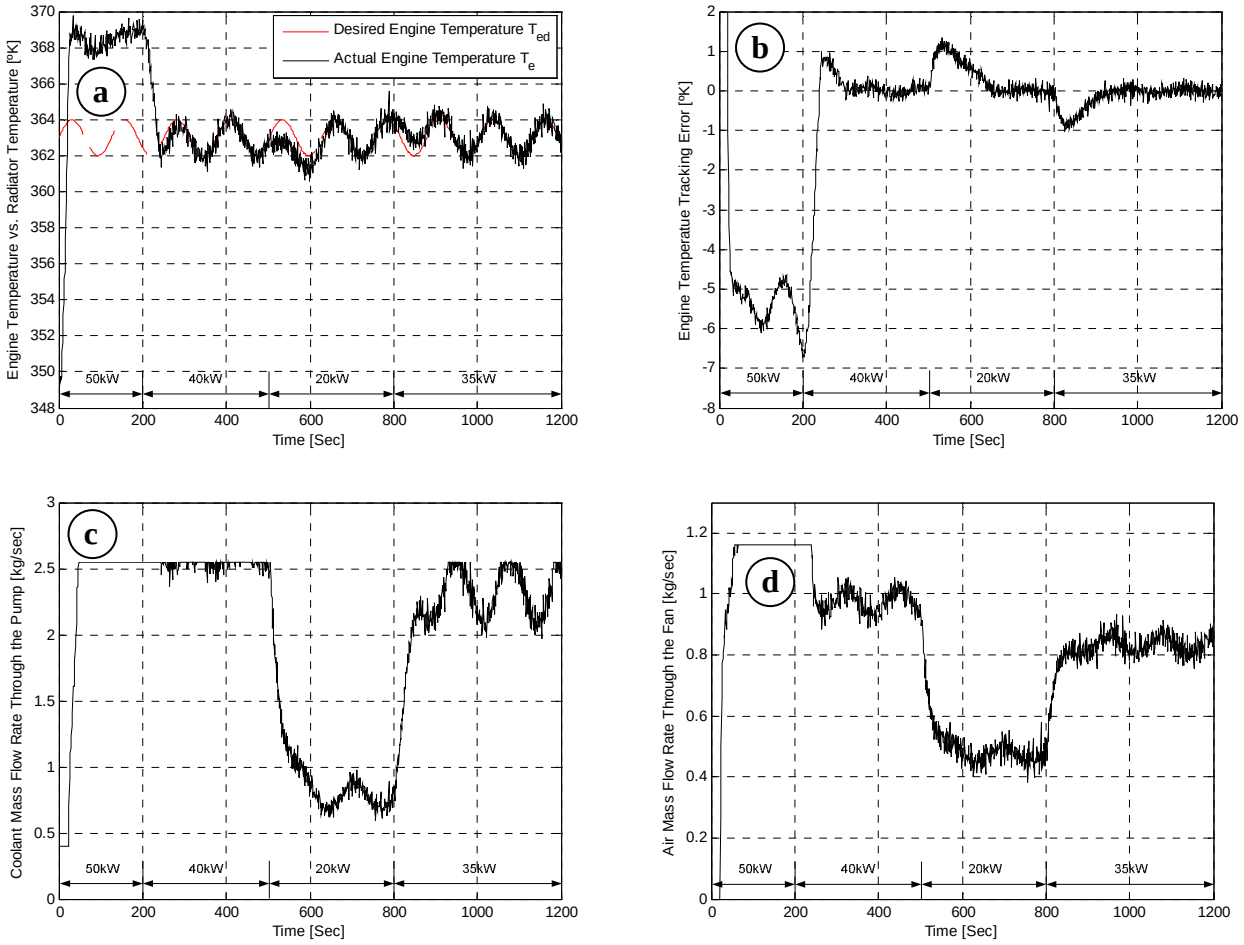

Figure 6: Numerical response of the normal radiator operation for variable engine thermal loads. (a) Simulated engine temperature response for desired engine temperature profile $T_{ed}(t) = 363 + \sin(0.05t)$ °K; (b) Simulated engine commanded temperature tracking error; (c) Simulated mass flow rate through the pump; and (d) Simulated air mass flow rate through the radiator fan.

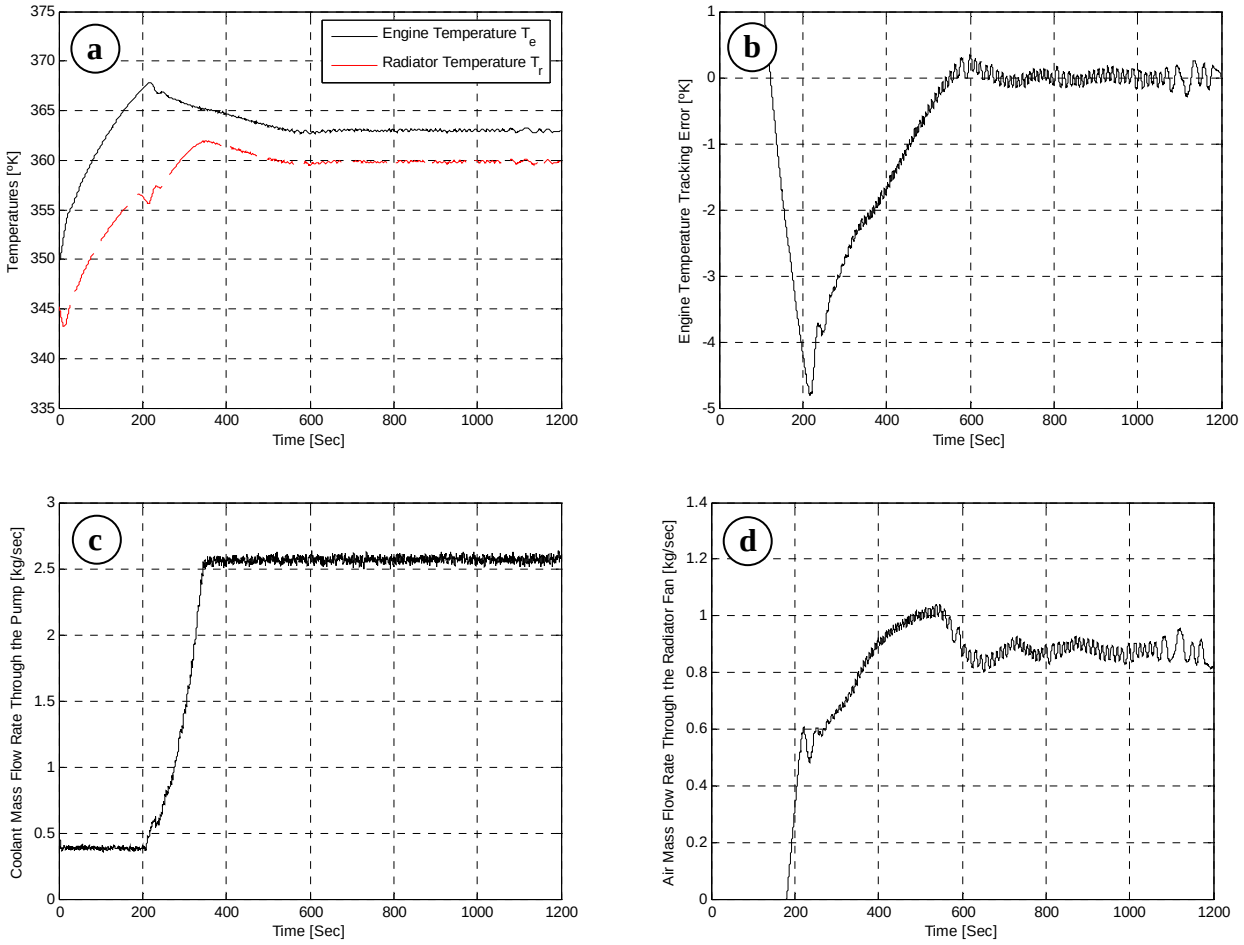

Figure 7: First experimental test results for the normal radiator operation controller with emulated vehicle speed of 20km/h and $Q_{in}(t) = 35\,\text{kW}$. (a) Experimental engine and radiator temperatures with a desired engine temperature $T_{ed}(t) = 363\,^{o}\text{K}$; (b) Experimental engine temperature tracking error; (c) Experimental coolant mass flow rate through the pump; and (d) Experimental air mass flow rate through the radiator fan.

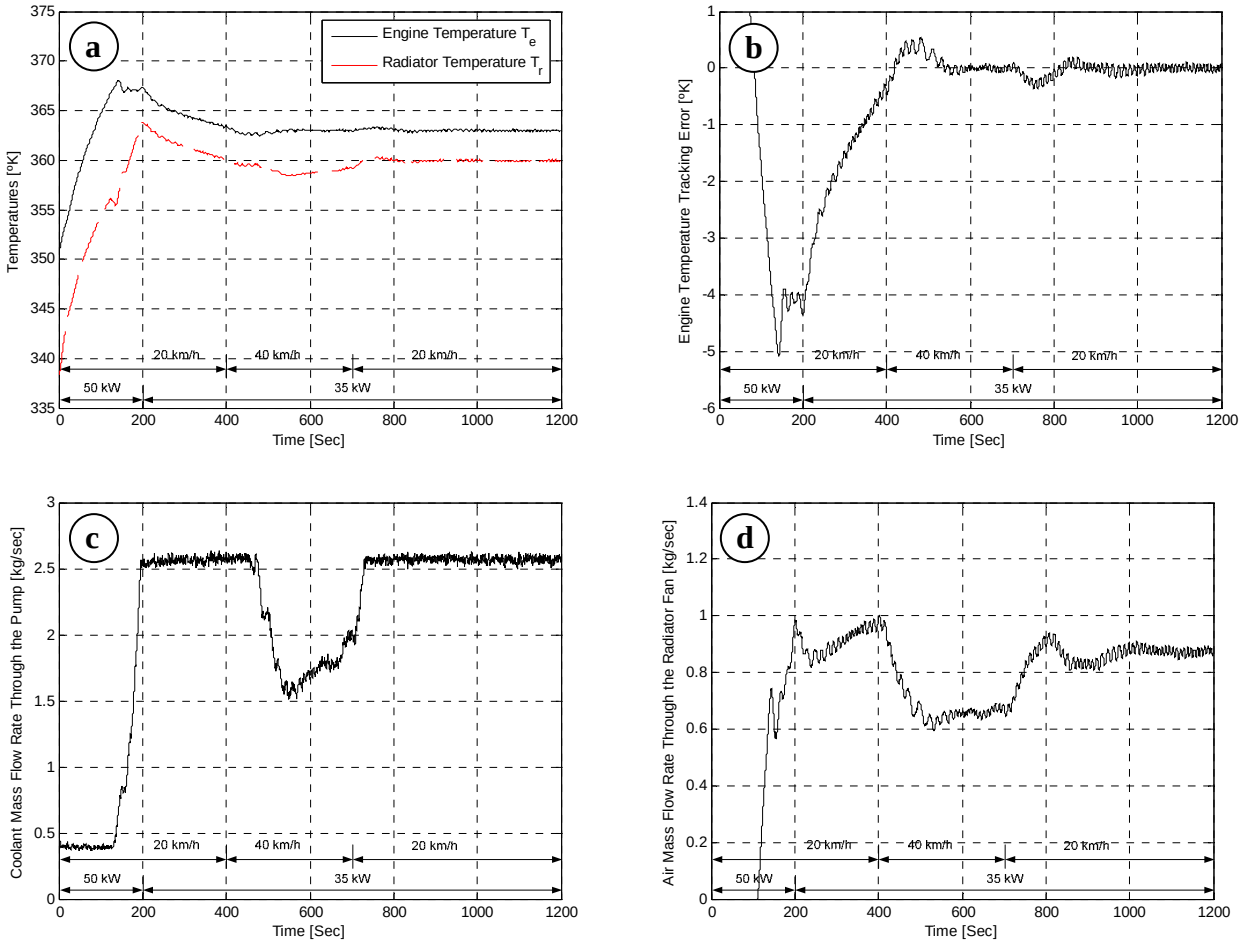

Figure 8: Second experimental test scenario for the normal radiator operation controller where the input heat and ram air disturbance vary with time. (a) Experimental engine and radiator temperatures with a desired engine temperature $T_{ed}(t) = 363\,^{o}\mathrm{K}$; (b) Experimental engine temperature tracking error; (c) Experimental coolant mass flow rate through the pump; and (d) Experimental air mass flow rate through the radiator fan.

The simulation and experimental results are summarized in Table 1 to compare the controller strategies. To ensure uniform operating conditions, all reported data corresponds to the first scenario thermal conditions. Further, the controller gains, initial conditions, and temperature set points were maintained for both the simulation and experimental tests. Note that adaptive and robust controllers were also designed and implemented (Salah *et al.*, 2006) for comparison purposes. However, the designs are not reported in this paper. For these two controllers, the radiator temperature set point was required which may be considered a weakness.

Overall, the normal radiator operation strategy was better than the adaptive and robust control strategies. However, it is not as good as the backstepping control when compared in terms of power consumption despite achieving less temperature tracking error. Therefore, the backstepping robust control strategy is considered to be the best among all controllers and operation strategies. The power measure is the minimum, the heat change handling is more satisfactory, and a set point for the radiator temperature is not required. From Table 1, it is clear that the variations in the actual coolant temperature about the set point, quantified by the steady state tracking error, are relatively minor given that the maximum absolute tracking error is 0.3% (*e.g.*, adaptive control).

Remark 5: The power measure $P_M = \frac{1}{T}\int_{t_o}^{t}\left[\frac{1}{2\rho_c^2 A_c^2}\dot{m}_c^3(\tau)+\frac{1}{2\rho_f^2 A_f^2}\dot{m}_f^3(\tau)+P_v\right]d\tau$ calculates the average power consumed by the system actuators over the time *T=20min*. Power measure is performed for the duration of the experimental test (*T*) using the trapezoidal method of integration. The power consumed by the smart valve is considered to be quite small so it is neglected. The following parameters' values are used: ρ_c = 1000kg/m^3, ρ_a = 1.2kg/m^3, A_c = 1.14mm^2, A_a = 114mm^2, and $P_v \cong 0$.

Description	Error $\lvert e_{ss}\rvert$ [^{o}K]		Power P_M [W]	
	Simulation	Experiment	Simulation	Experiment
Backstepping robust control	0.616	0.695	15.726	16.449
Normal radiator operation strategy	0.105	0.175	18.922	19.334
Adaptive control	1.003	1.075	18.646	18.880
Robust control	0.905	0.935	17.079	17.795

Table 1: Simulation and experimental results summary for four control strategies

6. CONCLUSION

Advanced automotive thermal management system can have a positive impact on gasoline and diesel engine cooling systems. In this paper, a suit of servo-motor based-cooling system components have been assembled and controlled using a Lyapunov-based nonlinear control technique. The control algorithm has been investigated using both simulation and

experimental tests. Two detailed and two supplemental controllers were applied to regulate the engine temperature. In each instance, the controllers successfully maintained the engine block to setpoint temperatures with small error percentages. It has also been shown that the power consumed by the system actuators can be reduced. Overall, the findings demonstrated that setpoint temperatures can be maintained satisfactory while minimizing power consumption which ultimately impacts fuel economy.

ACKNOWLEDGEMENTS

The authors would like to thank the U.S. Army Tank-Automotive and Armaments Command (TACOM), and the Automotive Research Center (ARC) at the University of Michigan and Clemson University for funding this project.

REFERENCES

Brace, C., Burnham-Slipper, H., Wijetunge, R., Vaughan, N., Wright, K., and Blight, D., "Integrated Cooling Systems for Passenger Vehicles," SAE technical paper No. 2001-01-1248, 2001.

Chalgren, Jr, R., and Allen, D., "Light Duty Diesel Advanced Thermal Management," SAE technical paper No. 2005-01-2020, 2005.

Chalgren, Jr, R., and Barron, Jr, L., "Development and Verification of a Heavy Duty 42/14V Electric Powertrain Cooling System," SAE technical paper No. 2003-01-3416, 2003.

Chalgren, Jr, R., and Traczyk, T., "Advanced Secondary Cooling Systems for Light Trucks," SAE technical paper No. 2005-01-1380, 2005.

Chanfreau, M., Joseph, A., Butler, D., and Swiatek, R., "Advanced Engine Cooling Thermal Management System on a Dual Voltage 42V-14V Minivan," SAE technical paper No. 2001-01-1742, 2001.

Cho, H., Jung, D., Filipi, Z., and Assanis, D., "Application of Controllable Electric Coolant Pump for Fuel Economy and Cooling Performance Improvement," proceedings of the ASME IMECE, Advanced Energy Systems Division, vol. 44, pp. 43-50, Anaheim, CA, November 2004.

Choukroun, A., and Chanfreau, M., "Automatic Control of Electric Actuators for an Optimized Engine Cooling Thermal Management," SAE technical paper No. 2001-01-1758, 2001.

Cipollone, R., and Villante, C., "Vehicle Thermal Management: A Model-Based Approach," proceedings of the ASME Internal Combustion Engine Division, pp. 85-95, Long Beach, CA, October 2004.

Eberth, J., Wagner, J., Afshar, B., and Foster, R., "Modeling and Validation of Automotive "Smart" Thermal Management System Architecture," SAE technical paper No. 2004-01-0048, 2004.

Henry, R., Koo, J., and Richter, C., "Model Development, Simulation and Validation, of Power Train Cooling System for a Truck Application," SAE paper No. 2001-01-1731, 2001.

Page, R., Hnatczuk, W., and Kozierowski, J., "Thermal Management for the 21st Century – Improved Thermal Control & Fuel Economy in an Army Medium Tactical Vehicle," SAE paper No. 2005-01-2068, 2005.

Qu, Z., "Robust Control of Nonlinear Uncertain Systems," John Wiley & Sons, 1998.

Redfield, J., Surampudi, B., Ray, G., Montemayor, A., Mckee, H., Edwards, T., and Lasecki, M., "Accessory Electrification in Class 8 Tractors," SAE paper No. 2006-01-0215, 2006.

Salah, M., Wagner, J., and Dawson, D., "Adaptive and Robust Tracking Control for Thermal Management Systems," Clemson University CRB Technical Report, CU/CRB/10/2/06/#1, http://www.ces.clemson.edu/ece/crb/publictn/tr.htm, October 2006.

Setlur, P., Wagner, J., Dawson, D., and Marotta, E., "An Advanced Engine Thermal Management System: Nonlinear Control and Test", *IEEE/ASME Transactions on Mechatronics*, vol. 10, no. 2, pp. 210-220, April 2005.

Wagner, J., Marotta, E., and Paradis, I., "Thermal Modeling of Engine Components for Temperature Prediction and Fluid Flow Regulation", SAE technical paper No. 2001-01-1014, 2001.

Wagner, J., Ghone, M., Dawson, D., and Marotta, E., "Coolant Flow Control Strategies for Automotive Thermal Management Systems," SAE technical paper No. 2002-01-0713, 2002.

Wagner, J., Srinivasan, V., and Dawson, D., "Smart Thermostat and Coolant Pump Control for Engine Thermal Management Systems," SAE technical paper No. 2003-01-0272, 2003.

Wambsganss, M., "Thermal Management Concepts for Higher-Efficiency Heavy Vehicle," SAE technical paper No. 1999-01-2240, 1999.

APPENDIX A: Proof of Theorem 1

Let $V(z,t) \in \Re$ denote the non-negative function

$$V \triangleq \frac{1}{2} C_e e^2 + \frac{1}{2} C_r \eta^2 \tag{A.1}$$

where $z(t) \in \Re^2$ is defined as

$$z \triangleq \begin{bmatrix} e & \eta \end{bmatrix}^T. \tag{A.2}$$

Note that (A.1) is bounded as (refer to Theorem 2.14 of Qu (1998))

$$\lambda_1 \|z(t)\|^2 \leq V(z,t) \leq \lambda_2 \|z(t)\|^2 \tag{A.3}$$

where λ_1, and λ_2 are positive constants. After taking the time derivative of (A.1), then

$$\dot{V} = eN_{ed} + e\tilde{N}_e - eu_e - eM\eta + \eta N_{rd} + \eta \tilde{N}_r + \eta u_r - \eta C_r \dot{T}_{vr} \tag{A.4}$$

where (16) was utilized. From Appendix B, an expression for $\eta(t) C_r \dot{T}_{vr}(t)$ becomes

$$\eta C_r \dot{T}_{vr} = \frac{1}{2}\left[1 + \operatorname{sgn}(u_e)\right] x, \qquad x = \eta C_r \left(\beta_1 N_e - \beta_2 e - \beta_3 \eta\right) \tag{A.5}$$

where β_1, β_2, and β_3 are defined in (B.3). From (A.5), it is clear that $\eta(t) C_r \dot{T}_{vr}(t)$, introduced in (A.4), changes with respect to the sign of the control input $u_e(t)$. Consequently, two cases are realized.

<u>Case I:</u> $\eta(t) C_r \dot{T}_{vr}(t) = 0$ **when** $u_e(t) \in (-\infty, 0)$

The expression of $\dot{V}(t)$, introduced in (A.4), can be rewritten as

$$\dot{V} = eN_{ed} + e\tilde{N}_e - K_e e^2 + \eta N_{rd} + \eta \tilde{N}_r - K_r \eta^2 + eM\eta \tag{A.6}$$

where (20) and (21) were utilized. To facilitate the subsequent analysis, the auxiliary signals $\tilde{N}_e(T_e, t)$ and $\tilde{N}_r(T_e, T_r, t)$, introduced in (17) can be computed as

$$\tilde{N}_e = -Me \tag{A.7}$$

$$\tilde{N}_r = -Me - M\eta \tag{A.8}$$

where (18) and (19) were used as well as M introduced in (11). Application of (A.7), (A.8), and the triangle inequality allows $\dot{V}(t)$ to be upper bounded as

$$\dot{V} \le -K_e|e|^2 - K_r|\eta|^2 + |e|N_{ed}| - M|e|^2 + |\eta|N_{rd}| - M|\eta|^2 . \tag{A.9}$$

By using (A.2) and completing the squares for the last four terms on the right-hand side of (A.9), the following inequality can be obtained (Qu, 1998) as

$$\dot{V} \le -\lambda_3 \|z\|^2 + \varepsilon_o \tag{A.10}$$

where $\lambda_3 = \min\{K_e, K_r\}$ and $\varepsilon_o \triangleq \frac{|N_{ed}|^2}{4M} + \frac{|N_{rd}|^2}{4M}$. From (A.1), (A.3), and (A.10), then $V(z,t) \in L_\infty$; hence, $e(t), \eta(t), z(t) \in L_\infty$. From (10) and Assumption 4, $T_e(t) \in L_\infty$ since $e(t), \eta(t) \in L_\infty$ and $u_e(t), u_r(t) \in L_\infty$ based on (20) and (21). Thus, $T_{vr}(t) \in L_\infty$ can be realized using (15) in Remark 2 and the relation $T_{vr} = T_{vro} + \overline{T}_{vr}$. From the previous bounding statements, $T_r(t), \dot{m}_r(t), H(t), \dot{m}_c(t), \dot{m}_f(t) \in L_\infty$ since $\dot{m}_r = m_o + \overline{m} = H_o \dot{m}_c + \overline{H}\dot{m}_c$ and the information in (10), (15), and (16).

<u>Case II:</u> $\eta(t) C_r \dot{T}_{vr}(t) \neq 0$ **when** $u_e(t) \in [0, \infty)$

The expression of $\dot{V}(t)$, introduced in (A.4), can be rewritten as

$$\dot{V} = eN_{ed} + e\tilde{N}_e - K_e e^2 + \eta N_r - K_r \eta^2 - \eta C_r \beta_1 N_e + eM\eta - K_e \frac{C_r}{C_e} e\eta \tag{A.11}$$

where (17), (20), (21), and (A.5) were applied. For convenience, the expression in (A.11) may be rewritten as

$$\dot{V} = -K_e e^2 - K_r \eta^2 + e\tilde{N}_e + eN_{ed} + \eta \tilde{N} + \eta N_d + eM\eta - K_e \frac{C_r}{C_e} e\eta \tag{A.12}$$

where the auxiliary signal $\tilde{N}(T_e, T_r, t)$ becomes

$$\tilde{N} \triangleq N - N_d . \tag{A.13}$$

The variables $N(T_e, T_r, t)$ and $N_d(t)$ are defined as

$$N \triangleq N_r - C_r \beta_1 N_e \tag{A.14}$$

$$N_d \triangleq N\Big|_{T_e = T_{ed}, T_r = T_{vr}} = N_{rd} - C_r \beta_1 N_{ed} \tag{A.15}$$

where $N_e(t), N_r(t), N_{ed}(t)$ and $N_{rd}(t)$ were introduced in (18), (19), and β_1 was introduced in (B.3). The auxiliary signal $\tilde{N}(T_e, T_r, t)$, introduced in (A.13), can be computed as

$$\tilde{N} = -\left(M - K_e \frac{C_r}{C_e} \right) e - M\eta \tag{A.16}$$

based on (17), (18), (19), and (B.3). By utilizing (A.7), (A.16), and the triangle inequality, $\dot{V}(t)$ in (A.12) can be upper bounded as

$$\dot{V} \le -K_e |e|^2 - K_r |\eta|^2 + |e| |N_{ed}| - M|e|^2 + |\eta| |N_d| - M|\eta|^2 . \tag{A.17}$$

The final step of the proof follows the same argument presented in Case I to demonstrate that $\dot{V} \le -\lambda_3 \|z\|^2 + \varepsilon_o$ and all signals are bounded where $\varepsilon_o \triangleq \frac{|N_{ed}|^2}{4M} + \frac{|N_d|^2}{4M}$.

APPENDIX B: Finding $C_r \dot{T}_{vr}$ Expression

The expression for $C_r T_{vr}$ can be written as

$$C_r T_{vr} = \begin{Bmatrix} C_r T_{vro} & , \quad \forall u_e \in (-\infty, 0) \\ C_r T_{vro} + \dfrac{C_r u_e}{M}, & \forall u_e \in [0, \infty) \end{Bmatrix} \tag{B.1}$$

where (15) and the relation $T_{vr} = T_{vro} + \bar{T}_{vr}$ were utilized. The parameter M was introduced in (11). After taking the first time derivative of (B.1), the following expression can be obtained

$$C_r \dot{T}_{vr} = \begin{Bmatrix} 0 & , \quad \forall u_e \in (-\infty, 0) \\ C_r (\beta_1 N_e - \beta_2 e - \beta_3 \eta), & \forall u_e \in [0, \infty) \end{Bmatrix} \tag{B.2}$$

where (16), (17), and (20) were applied. The coefficients β_1, β_2 and β_3 are defined as

$$\beta_1 \triangleq \frac{K_e}{MC_e}, \quad \beta_2 \triangleq \frac{K_e^2}{MC_e}, \quad \beta_3 \triangleq \frac{K_e}{C_e}. \tag{B.3}$$

APPENDIX C: Nomenclature List

A_a	fan blowing area [m^2]
A_c	pump outlet cross section area [m^2]
A_f	frontal area of the fan [m^2]
A_p	area of valve plate [m^2]
α_e	positive control gain
b	water pump inlet impeller width [m]
b_f	fan damping coefficient [N.m.s/Rad]
b_p	pump damping coefficient [N.m.s/Rad]
b_v	valve damping coefficient [N.m.s/Rad]
β	inlet impeller angel [Rad]
β_r	positive constant [Rad/sec.m^2]
C_e	engine block capacity [kJ/ºK]
C_{pc}	coolant specific heat [kJ/kg.ºK]
C_{pa}	air specific heat [kJ/kg.ºK]
C_r	radiator capacity [kJ/ºK]
c	coulomb friction [N]
d	gear pitch [m]
ΔP	pressure drop across the valve [Pascal]
e	engine temperature tracking error [ºK]
e_o	initial engine temperature tracking error [ºK]
e_{ss}	engine temperature steady state error [ºK]
ε	effectiveness of the radiator fan [%]
η	radiator temperature tracking error [ºK]
η_f	radiator fan efficiency [%]
h	valve piston translational displacement [m]
H	normalized valve position [%]
$\overline{H}$	normalized valve position for $\overline{m}$ [%]
H_o	minimum normalized valve position [%]
i_{af}	radiator fan motor armature current [A]
i_{ap}	water pump motor armature current [A]
i_{av}	valve motor armature current [A]
J_f	radiator fan and load inertia [kg.m^2]
J_p	water pump and load inertia [kg.m^2]
J_v	valve and load inertia [kg.m^2]
K_{bf}	radiator fan back EMF constant [V.sec/Rad]
K_{bp}	water pump back EMF constant [V.sec/Rad]
K_{bv}	valve back EMF constant [V.sec/Rad]
K_e	positive control gain
K_{mf}	radiator fan torque constant [N.m/A]
K_{mp}	water pump torque constant [N.m/A]
K_{mv}	valve torque constant [N.m/A]
K_r	positive control gain
L_{af}	radiator fan inductance [H]
L_{ap}	water pump inductance [H]
L_{av}	valve inductance [H]
$\overline{m}$	additional coolant mass flow rate control input for m_o in radiator [kg/sec]
$\dot{m}_c$	pump coolant mass flow rate [kg/sec]
$\dot{m}_f$	fan air mass flow rate [kg/sec]
m_o	min. radiator coolant mass flow rate [kg/sec]
$\dot{m}_r$	radiator coolant mass flow rate [kg/sec]
$\dot{m}_{raw}$	ram air mass flow rate [kg/sec]
M_1	pump coolant mass flow rate meter
M_2	radiator fan air mass flow rate meter
N	worm to valve gear ratio
P_1	valve power sensor
P_2	water pump power sensor
P_3	radiator fan power sensor
P_M	cooling system power measure [W]
P_{sys}	cooling system power consumption [W]
P_v	valve power consumption [W]
ρ_a	air density [kg/m^3]
ρ_c	coolant density [kg/m^3]
ρ_e	positive constant
Q_{in}	combustion process heat energy [kW]
Q_o	radiator heat lost due to uncontrollable air flow [kW]
r	pump inlet to impeller blade length [m]
R_{af}	radiator fan resistor [Ohm]
R_{ap}	water pump resistor [Ohm]
R_{av}	valve resistor [Ohm]
R_f	radiator fan radius [m]
sgn	standard signum function
t_o	initial time [sec]
T_1	coolant temperature at engine outlet [ºK]
T_2	coolant temperature at radiator outlet [ºK]

T_3 ambient temperature sensor [ºK]
T_e coolant temperature at the engine outlet [ºK]
T_∞ surrounding ambient temperature [ºK]
T_r radiator outlet coolant temperature [ºK]
θ_v valve angular displacement [Rad]
T_{ed} desired engine temperature trajectory [ºK]
T_{vr} design virtual radiator reference temp. [ºK]
T_{vro} virtual radiator reference temperature design constant [ºK]
$\overline{T}_{vr}$ control input that affects the radiator loop mass flow rate [ºK]
v inlet radial coolant velocity [m/sec]
V_{af} air volume per fan rotation [m^3/Rad]
V_o fluid volume per pump rotation [m^3/Rad]
V_f voltage applied on the radiator fan [V]
V_p voltage applied on the pump [V]
V_v voltage applied on the valve [V]
ω_f radiator fan angular velocity [Rad/sec]
ω_p water pump angular velocity [Rad/sec]